

## STANDARD FINITE VOLUME THEORY APPLIED TO TOPOLOGY OPTIMIZATION FOR COMPLIANCE MINIMIZATION OF CONTINUUM ELASTIC STRUCTURES

**Marcelo Vitor Oliveira Araujo**

**Eduardo Nobre Lages**

**Marcio André Araújo Cavalcante**

*marcelo.vitor.o.a@gmail.com*

*enl@lccv.ufal.br*

*marcio.cavalcante@ctec.ufal.br*

*Federal University of Alagoas*

*Av. Lourival Melo Mota, S/N, Tabuleiro do Martins, Maceió, 57072-900, Alagoas, Brazil.*

**Abstract.** In topology optimization of structures, the objective is to establish the best material distribution inside of an analysis domain given an objective function, as compliance minimization, and mechanical restriction to the problem. Normally, in the gradient-based topology optimization algorithms, there are some problems related to numerical instabilities, such as checkerboard pattern, mesh dependence and local minima. The checkerboard effect is directly related to the assumptions of the finite element method, as the satisfaction of equilibrium equations and continuity conditions through the nodes. On the other hand, the finite volume theory satisfies the equilibrium equations at the subvolume level, and the static and kinematic continuities are established through adjacent subvolumes interfaces, as expected from the continuum mechanics point of view. To solve the problems related to the checkerboard and mesh dependence in the finite element method, it is often recommended the use of sensitivity or perimeter control filters. For the finite volume theory, the sensitivity filter is employed with the purpose to control better the mesh dependence and length scale numerical issues. Comparisons of the optimum topologies and computational performances of the analyzed approaches are presented, demonstrating the influence of the adopted numerical method on the obtaining optimal solution when a filtering technique is employed.

**Keywords:** Finite Volume Theory, Topology Optimization, Sensitivity Filters, Continuum Elastic Structures, Compliance Minimization.

## 1 Introduction

In the design of structure, there is a need to find the best project that attends all restrictions and optimizes the material distribution in the given domain. Normally, this “optimal project” is accomplished taking advantage of engineer experience, which causes a dependence of their work. As a result, structural optimization techniques have been developed to help engineers finding the optimal configuration for structures, with no need to base their projects only on past experiences.

In general, the structural optimization methods are divided in two prime categories: material optimization and material distribution optimization. The first category pretends to find the best material properties, while the second seeks to find the best material distribution in the analysis domain. These methods can be divided in three subcategories: sizing optimization, which seeks to find optimal size of the structures, in terms of length, thickness and highness; shape optimization, which introduces shape changes to obtain the optimum design; and topology optimization, which seeks to find the best material distribution inside a given domain attaining the objective function and problem constraints.

Topology optimization is a method proposed initially by Michell [1], who derived the Optimality Criteria (OC) method for the least weight layout of trusses. This method is typically used for compliance minimization or stiffness maximization problems. According to Bendsøe and Sigmund [2], the interest of topology optimization is to define which points of the domain must be material or void, generating what is called “black and white” design. In this case, there is a binary “0-1” problem, where the optimal solution is given by the union of each element with the value 1, leading to problems of discrete optimization.

The actual material distribution is described in terms of a continuum function, which defines the material relative density and assumes any real value between approximately 0, indicating void, and 1 indicating solid. To penalize the intermediate values, it can be applied the SIMP (Solid Isotropic Material with Penalization) method. In this case, the material properties are assumed as constants inside each element of the discretized analysis domain, and the design variables are element relative density. Therefore, the properties are modeled by the material relative density power a designated exponent with the objective to penalize the intermediate values.

The topology optimization is a powerful and robust method to the design of structures, however there are some difficulties related to numerical instabilities. According to Sigmund and Petersson [3], there are three categories of numerical problems: checkerboard pattern, which refers to the formation of regions that alternate solid element and void elements ordered as a checkerboard; mesh dependency, which refers to the problem of qualitatively different solutions to different structure discretizations; and local minima, which refers to the problem of different solutions to the same discretization problem when different initial parameters are adopted. Therefore, it is undesirable to have any of these numerical instabilities.

To solve these numerical instabilities usually, it is proposed the adoption of higher order elements Sigmund and Peterson [3] and Díaz and Sigmund [4], or filtering techniques based on image processing Sigmund [5]. In the image filter, the sensitivity of each element depends on the weight average of the neighboring elements. This procedure can help to solve the problems associated with checkerboard and mesh dependence problems, as suggested by Sigmund and Petersson [3].

Another numerical issue is the local minima, which is related to the fact that the gradient-based algorithms can encounter problems to find the global minimum, once small changes in the simulation parameters can lead to local minimum instead of a global minimum solution, Christensen and Klarbring [6]. Basically, this occurs due to the loss of convexity when a value bigger than one is applied as the density penalty factor. To solve this mentioned problem, Christensen and Klarbring [6] suggested the adoption of the continued penalization scheme, where a gradually increase of the density penalty factor is employed during the optimization process. However, this does not guarantee that the solution found is a global minimum, but, with it, the solution is unique, that is, the optimum solution does not vary with the starting point, Christensen and Klarbring [6].

Numerical methods for topology optimization have been extensively investigated since 1980s,

Rozvany [7], basically, it may be highlighted the landmark paper of Bendsøe and Kikuchi [8]. Certainly, the finite element method is the most common technique for numerical analysis in topology optimization. As a result, its advantages and disadvantages are well known. Basically, this method subdivides the analysis domain in smaller subdomains that have simpler geometric shape. Therefore, the differential equilibrium equations can be solved by a linear system of equations that describes the linear behavior of the discretized domain.

An alternative technique to the finite element method is the finite volume theory, proposed initially by Bansal and Pindera [9]. According to Cavalcante [10], this technique uses the volumetric means of the fields that define the material behavior, and imposes the boundary and continuity conditions in an average sense, related to tractions and displacements. This technique has shown to be a method adequate to the elastic analysis of tensions, comparison results using this theory with analytic solutions and the finite element analysis demonstrated the efficiency of this method, see Cavalcante et al. [11,12,13] and Cavalcante and Pindera [14,15].

Actually, the numerical instabilities, presented previously, are directly related to the topology optimization problem, specifically the mesh dependency and the local minima. However, the checkerboard topology optimization numerical problem is directly associated with the assumptions of the finite element method, employed during the optimization process. Basically, it forces the satisfaction of equilibrium equations and compatibility conditions only in the nodes of each finite element of the discretized domain. In addition, the equilibrium equations are not satisfied at element level, being satisfied only when a sufficiently fine mesh is employed.

On the other hand, the finite volume theory satisfies the equilibrium equations at the subvolume level and the compatibility conditions are established through the subvolume interfaces. Therefore, in the finite volume theory the connections between adjacent subvolumes occurs through its interfaces, which is more likely from the continuum mechanics point of view. At the same time, in the finite element method the connections between neighboring elements occur through the nodes, leading to optimum topologies with the presence of checkerboard regions.

This paper addresses a new approach for topology optimization based on the standard finite volume theory for compliance minimization problems and employing a sensitivity filtering, pretending to overcome numerical problems as checkerboard pattern and mesh dependence. Comparison results obtained by the topology optimization approach based on the finite volume theory with the same approach based on the finite element method proves the efficiency of the proposed approach. In addition, the results, for some examples, show that the optimum topologies obtained by the finite volume theory are stiffer than the ones obtained by the finite element method, which demonstrates its efficiency.

## **2 Finite volume theory**

The finite volume method is a well-known numerical method for the solution of boundary values problems in the fluid mechanics, Versteeg and Malalasekera [16]. The satisfaction of the governing field equations within subvolumes of the discretized domain of interest in an integral sense is a key feature of the finite volume method which distinguishes it from the variational technique such as the finite element method, Cavalcante et al. [17]. The simplicity and demonstrated stability of finite volume method in the solution of problems in fluid mechanics have motivated the application of this technique in solid mechanic problems. Therefore, there are three versions of this technique in the analysis of solid mechanic problems. The first two have been developed to lead with homogeneous materials and structures, while the third version evolved independently and nearly in parallel for applications involving heterogeneous materials.

The finite volume theory, denomination originally suggested by Bansal [18] and Cavalcante [10], has its roots in the so-called higher-order theory for functionally graded materials, which was developed in a sequence of papers during the 1990's and summarized in Aboudi et al. [19]. According to Bansal and Pindera [9], the prime changes involve the simplification of the domain discretization and the substitution of the volumetric average of the displacement and stress field for average quantities associated to each cell interface. Therefore, this theory presents some similarities with the

finite volume method, usually applied for fluid mechanics, for this reason was suggested the adaptation for its denomination for finite volume theory.

The first to work to suggest this simplification to the higher-order theory was Bansal and Pindera [9], followed by Cavalcante [10] and Cavalcante et al. [11,12] that contributed with a bidimensional parametric formulation more appropriated for thermal-mechanic analysis of curved structures. After this, Gattu et al. [20] and Khatam and Pindera [21,22] followed Cavalcante et al. [11,12], introducing a parametric mapping to the homogenized version of the finite volume theory, known as FVDAM (finite volume direct averaging micromechanics). A generalization for homogenized version of the finite volume theory for periodic materials subject to finite deformations was presented by Cavalcante and Pindera [23,24]. On the same way, Cavalcante and Pindera [14,15] presented the generalized finite volume theory, incorporating besides average displacements, rotations and curvatures to the mechanical formulation for elastic analysis of solids.

Basically, this technique employs the volume average of the different fields that define the material behavior and imposes boundary and continuity conditions between adjacent subvolumes in an average-sense. In addition, the equilibrium equations are satisfied in an averaged-sense in the subvolume, and the displacement filed in the subvolume is modeled by second-order polynomials defined by local coordinates.

## 2.1 Standard formulation of the finite volume theory

The formulation presented here has its bases in the zeroth order Cartesian formulation for bidimensional structures of the finite volume theory presented by Calcante and Pindera [14]. Figure 1 presents the adopted reference domain, in this case, it is considered a rectangular domain occupying the plane  $x_1 - x_2$ . This actual domain is discretized in  $N_\beta$  horizontal subvolumes and  $N_\gamma$  vertical subvolumes, designated by the  $(\beta, \gamma)$  ordinated par, as shown in Figure 1. The dimensions of each subvolume can be expressed by  $l_\beta$  and  $h_\gamma$  (for  $\beta = 1, \dots, N_\beta$  and  $\gamma = 1, \dots, N_\gamma$ ) at the axis  $x_1$  and  $x_2$ , respectively. Each subvolume can be designated by an unique integer value given by  $q = \beta + (\gamma - 1) \cdot N_\beta$ , which gives a total number of rectangular subvolumes for the discretized structures of  $N_q = N_\beta \cdot N_\gamma$ .

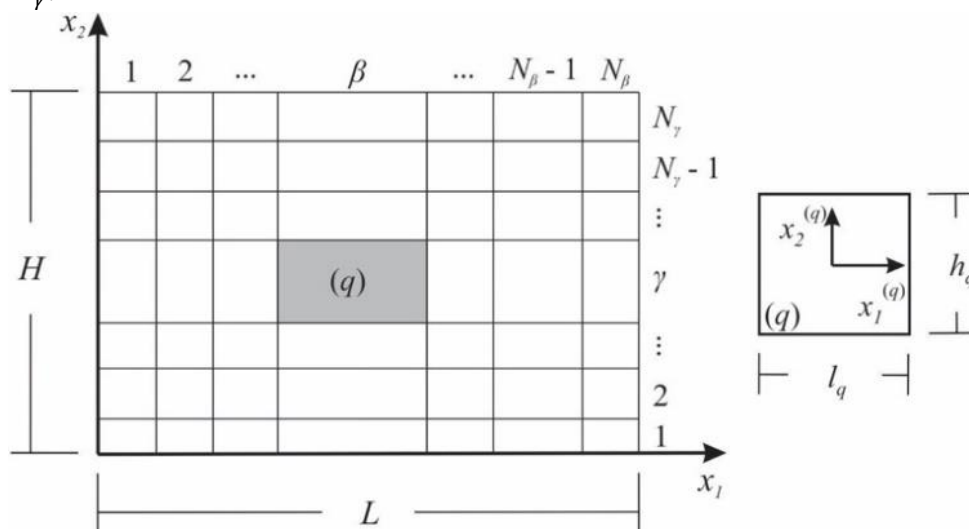


Figure 1. Discretized structure in rectangular subvolumes and local system of a generic subvolume.

The displacement field of a subvolume  $(\beta, \gamma)$  at the plane  $x_1 - x_2$  can be approximated by a second-order polynomials expressed as a function of the local coordinates inside each subvolume, Cavalcante and Pindera [14]. Therefore, these polynomials can be written as

$$u_i^{(q)} = W_{i(00)}^{(q)} + x_1^{(q)} W_{i(10)}^{(q)} + x_2^{(q)} W_{i(01)}^{(q)} + \frac{1}{2} \left( 3 \left( x_1^{(q)} \right)^2 - \frac{l_q^2}{4} \right) W_{i(20)}^{(q)} + \frac{1}{2} \left( 3 \left( x_2^{(q)} \right)^2 - \frac{h_q^2}{4} \right) W_{i(02)}^{(q)} \quad (1)$$

where  $i = 1, 2$  and  $W_{i(mn)}^{(q)}$  are unknown coefficients of the displacement field.

## 2.2 Local stiffness matrix

On this formulation, we need to calculate the surface-averaged values of the displacement field components, which are given by

$$\bar{u}_i^{(q,p)} = \frac{1}{l_q} \int_{-l_q/2}^{+l_q/2} u_i^{(q)} \left( x_1^{(q)}, \mp h_q/2 \right) dx_1^{(q)}, \text{ for } p = 1, 3. \quad (2)$$

$$\bar{u}_i^{(q,p)} = \frac{1}{h_q} \int_{-h_q/2}^{+h_q/2} u_i^{(q)} \left( \pm l_q/2, x_2^{(q)} \right) dx_2^{(q)}, \text{ for } p = 2, 4. \quad (3)$$

where  $\bar{u}_i^{(q,p)}$  are the surface-averaged displacements of a generic subvolume  $q$ , Figure 2(a).

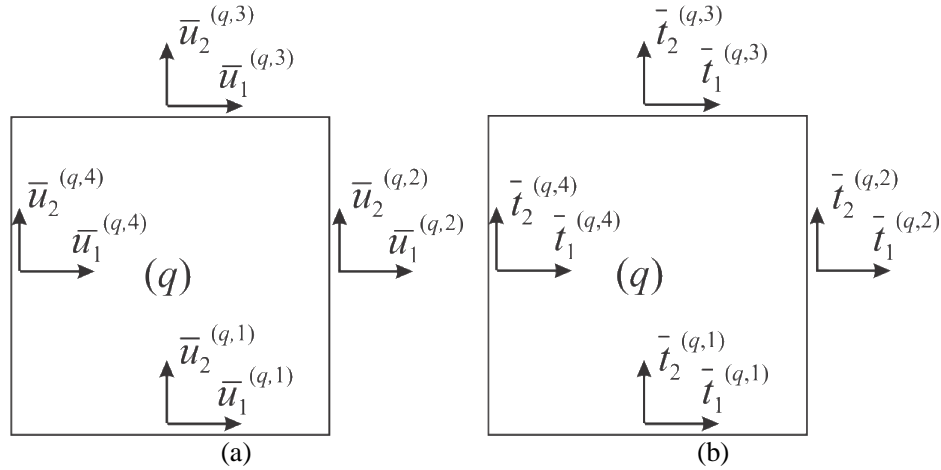


Figure 2. Surface averaged kinematic and static quantities for a generic subvolume  $q$ : (a) surface-averaged displacements and (b) surface-averaged tractions.

Using the components of the displacement field, presented in Eq. (1), in Eqs. (2) and (3), eight expressions can be obtained for the surface-averaged displacement as a function of the displacement field coefficients. Therefore, these expressions can be organized in matrix notation as follows:

$$\bar{\mathbf{u}}^{(q)} = \mathbf{A}_{(8 \times 8)}^{(q)} \mathbf{W}^{(q)} + \mathbf{a}_{(8 \times 2)}^{(q)} \mathbf{W}_{(00)}^{(q)} \quad (4)$$

where  $\bar{\mathbf{u}}^{(q)} = [\bar{u}_1^{(q,1)}, \bar{u}_2^{(q,1)}, \bar{u}_1^{(q,2)}, \bar{u}_2^{(q,2)}, \bar{u}_1^{(q,3)}, \bar{u}_2^{(q,3)}, \bar{u}_1^{(q,4)}, \bar{u}_2^{(q,4)}]^T$  is the surface-averaged displacement vector,  $\mathbf{W}^{(q)} = [W_{1(10)}^{(q)}, W_{1(01)}^{(q)}, W_{1(20)}^{(q)}, W_{1(02)}^{(q)}, \dots, W_{2(02)}^{(q)}]^T$  is the vector containing the first and second order coefficients of the displacement field and  $\mathbf{W}_{(00)}^{(q)} = [W_{1(00)}^{(q)}, W_{2(00)}^{(q)}]^T$  is the vector containing the zeroth order coefficients of the displacement field. The matrices  $\mathbf{A}_{(8 \times 8)}^{(q)}$  and  $\mathbf{a}_{(8 \times 2)}^{(q)}$  depend on the geometric features of the subvolume and are defined on the Appendix. Thus, the vector  $\mathbf{W}^{(q)}$  can be evaluated as function of  $\bar{\mathbf{u}}^{(q)}$  and  $\mathbf{W}_{(00)}^{(q)}$  as shown below

$$\mathbf{W}^{(q)} = \left( \mathbf{A}_{(8 \times 8)}^{(q)} \right)^{-1} \bar{\mathbf{u}}^{(q)} - \left( \mathbf{A}_{(8 \times 8)}^{(q)} \right)^{-1} \mathbf{a}_{(8 \times 2)}^{(q)} \mathbf{W}_{(00)}^{(q)} \quad (5)$$

Based on the aspects of the linear elasticity theory and modeling isotropic and homogeneous materials, the components of the traction vector can be acting on the faces of a generic subvolume  $q$  can be defined as

$$\bar{t}_i^{(q,p)} = \mp \frac{1}{l_q} \int_{-l_q/2}^{+l_q/2} \sigma_{2i} \left( x_1^{(q)}, \mp h_q/2 \right) dx_1^{(q)}, \text{ for } p = 1, 3 \quad (6)$$

$$\bar{t}_i^{(q,p)} = \pm \frac{1}{h_q} \int_{-h_q/2}^{+h_q/2} \sigma_{1i} \left( \pm l_q/2, x_2^{(q)} \right) dx_2^{(q)}, \text{ for } p = 2, 4 \quad (7)$$

Taking advantage of the elasticity theory for isotropic and homogeneous materials and substituting Eq. (1) in Eqs. (6) and (7), eight expressions are found, which can be organized in matrix notation as follows:

$$\bar{\mathbf{t}}^{(q)} = \mathbf{B}_{(8 \times 8)}^{(q)} \mathbf{W}^{(q)} \quad (8)$$

where  $\bar{\mathbf{t}}^{(q)} = \left[ t_1^{(q,1)}, t_2^{(q,1)}, t_1^{(q,2)}, t_2^{(q,2)}, t_1^{(q,3)}, t_2^{(q,3)}, t_1^{(q,4)}, t_2^{(q,4)} \right]^T$  is the surface-averaged traction vector for a generic subvolume  $q$ , Figure 2(b). The matrix  $\mathbf{B}_{(8 \times 8)}^{(q)}$  is defined in the Appendix.

Substituting Eq. (5) in Eq. (8), the traction vector  $\bar{\mathbf{t}}^{(q)}$  can be written as function of the surface-averaged displacement  $\bar{\mathbf{u}}^{(q)}$  as expressed below

$$\bar{\mathbf{t}}^{(q)} = \mathbf{B}_{(8 \times 8)}^{(q)} \left( \mathbf{A}_{(8 \times 8)}^{(q)} \right)^{-1} \bar{\mathbf{u}}^{(q)} - \mathbf{B}_{(8 \times 8)}^{(q)} \left( \mathbf{A}_{(8 \times 8)}^{(q)} \right)^{-1} \mathbf{a}_{(8 \times 2)}^{(q)} \mathbf{W}_{(00)}^{(q)} \quad (9)$$

Once in each face acts two different degrees of freedom for the zeroth order formulation, Eq. (9) can be rearranged as shown below

$$\begin{Bmatrix} \bar{\mathbf{t}}^{(q,1)} \\ \bar{\mathbf{t}}^{(q,2)} \\ \bar{\mathbf{t}}^{(q,3)} \\ \bar{\mathbf{t}}^{(q,4)} \end{Bmatrix} = \begin{bmatrix} \mathbf{B}_{(2 \times 8)}^{(q,1)} \\ \mathbf{B}_{(2 \times 8)}^{(q,2)} \\ \mathbf{B}_{(2 \times 8)}^{(q,3)} \\ \mathbf{B}_{(2 \times 8)}^{(q,4)} \end{bmatrix} \left( \mathbf{A}_{(8 \times 8)}^{(q)} \right)^{-1} \bar{\mathbf{u}}^{(q)} - \begin{bmatrix} \mathbf{B}_{(2 \times 8)}^{(q,1)} \\ \mathbf{B}_{(2 \times 8)}^{(q,2)} \\ \mathbf{B}_{(2 \times 8)}^{(q,3)} \\ \mathbf{B}_{(2 \times 8)}^{(q,4)} \end{bmatrix} \left( \mathbf{A}_{(8 \times 8)}^{(q)} \right)^{-1} \mathbf{a}_{(8 \times 2)}^{(q)} \mathbf{W}_{(00)}^{(q)} \quad (10)$$

or

$$\bar{\mathbf{t}}^{(q,p)} = \mathbf{B}_{(2 \times 8)}^{(q,p)} \left( \mathbf{A}_{(8 \times 8)}^{(q)} \right)^{-1} \bar{\mathbf{u}}^{(q)} - \mathbf{B}_{(2 \times 8)}^{(q,p)} \left( \mathbf{A}_{(8 \times 8)}^{(q)} \right)^{-1} \mathbf{a}_{(8 \times 2)}^{(q)} \mathbf{W}_{(00)}^{(q)} \quad (11)$$

where the superscript  $p$  indicates the face number inside the subvolume  $q$ .

In the absence of body forces, the satisfaction of the equilibrium conditions is achieved by the sum of the surface forces acting on the subvolume equal zero, as shown by

$$\mathbf{R}^{(q)} = \int_{S_q} \mathbf{t}^{(q)} dS_q = \mathbf{0}_{(2 \times 1)} \quad (12)$$

On this present formulation, the equilibrium equation for a generic subvolume can be expressed in terms of the surface-averaged traction vectors. Therefore, Eq. (12) can be converted by

$$\bar{\mathbf{t}}^{(q,1)} l_q + \bar{\mathbf{t}}^{(q,2)} h_q + \bar{\mathbf{t}}^{(q,3)} l_q + \bar{\mathbf{t}}^{(q,4)} h_q = \mathbf{0}_{(2 \times 1)} \quad (13)$$

or

$$\sum_{p=1}^4 \bar{\mathbf{t}}^{(q,p)} L_p^{(q)} = \mathbf{0}_{(2 \times 1)}. \quad (14)$$

where  $L_1^{(q)} = l_q$ ,  $L_2^{(q)} = h_q$ ,  $L_3^{(q)} = l_q$  and  $L_4^{(q)} = h_q$  are the face lengths of a subvolume.

Substituting Eq. (12) in Eq. (14), we arrive in the following equilibrium equation:

$$\left( \sum_{p=1}^4 \mathbf{B}_{(2 \times 8)}^{(q,p)} L_p^{(q)} \right) \left( \mathbf{A}_{(8 \times 8)}^{(q)} \right)^{-1} \bar{\mathbf{u}}^{(q)} - \left( \sum_{p=1}^4 \mathbf{B}_{(2 \times 8)}^{(q,p)} L_p^{(q)} \right) \left( \mathbf{A}_{(8 \times 8)}^{(q)} \right)^{-1} \mathbf{a}_{(8 \times 2)}^{(q)} \mathbf{W}_{(00)}^{(q)} = \mathbf{0}_{(2 \times 1)} \quad (15)$$

From Eq. (15), the vector  $\mathbf{W}_{(00)}^{(q)}$  can be written as

$$\mathbf{W}_{(00)}^{(q)} = \bar{\mathbf{a}}_{(2 \times 8)}^{(q)} \bar{\mathbf{u}}^{(q)} \quad (16)$$

where

$$\bar{\mathbf{a}}_{(2 \times 8)}^{(q)} = \left[ \left( \sum_{p=1}^4 \mathbf{B}_{(2 \times 8)}^{(q,p)} L_p^{(q)} \right) \left( \mathbf{A}_{(8 \times 8)}^{(q)} \right)^{-1} \mathbf{a}_{(8 \times 2)}^{(q)} \right]^{-1} \left( \sum_{p=1}^4 \mathbf{B}_{(2 \times 8)}^{(q,p)} L_p^{(q)} \right) \left( \mathbf{A}_{(8 \times 8)}^{(q)} \right)^{-1} \quad (17)$$

Combining Eqs. (5) and (16), we can find the following expression

$$\mathbf{W}^{(q)} = \bar{\mathbf{A}}_{(8 \times 8)}^{(q)} \bar{\mathbf{u}}^{(q)} \quad (18)$$

where  $\bar{\mathbf{A}}_{(8 \times 8)}^{(q)} = \left( \mathbf{A}_{(8 \times 8)}^{(q)} \right)^{-1} - \left( \mathbf{A}_{(8 \times 8)}^{(q)} \right)^{-1} \mathbf{a}_{(8 \times 2)}^{(q)} \bar{\mathbf{a}}_{(2 \times 8)}^{(q)}$ . Finally, replacing Eqs. (16) and (18) in Eq. (8), we find the local system of equations for a generic subvolume as

$$\bar{\mathbf{t}}^{(q)} = \mathbf{K}_{(8 \times 8)}^{(q)} \bar{\mathbf{u}}^{(q)} \quad (19)$$

where  $\mathbf{K}_{(8 \times 8)}^{(q)} = \mathbf{B}_{(8 \times 8)}^{(q)} \bar{\mathbf{A}}_{(8 \times 8)}^{(q)}$  is the local stiffness matrix for a generic subvolume  $q$ .

### 2.3 Global stiffness matrix assemblage

Following Araujo et al. [25], the global stiffness matrix of a structure, discretized by the zeroth order finite volume theory, is assembled considering the individual contribution of each subvolume and the global system of equations can be written as

$$\mathbf{T}_{(ndof \times 1)} = \mathbf{K}_{(ndof \times ndof)} \mathbf{U}_{(ndof \times 1)} \quad (20)$$

where  $ndof = 2N_\beta(N_\gamma + 1) + 2(N_\beta + 1)N_\gamma$  is the total number of degrees of freedom for the structure,  $\mathbf{U}_{(ndof \times 1)}$  and  $\mathbf{T}_{(ndof \times 1)}$  are global surface-averaged displacement vector and the global surface-averaged traction vector, respectively. Thus, the global stiffness matrix of the structure can be obtained by the following expression:

$$\mathbf{K}_{(ndof \times ndof)} = \sum_{q=1}^{N_q} \left[ \left( \mathbf{L}_{(8 \times ndof)}^{(q)} \right)^T \mathbf{K}_{(8 \times 8)}^{(q)} \mathbf{L}_{(8 \times ndof)}^{(q)} \right] \quad (21)$$

where  $\mathbf{L}_{(8 \times ndof)}^{(q)}$  is the structural kinematic compatibility matrix.

## 3 Topology optimization problem

The topology optimization problem consists on finding a subdomain  $\Omega_{opt}$ , with a limited volume  $\bar{V}$ , inside a pre-defined analysis domain  $\Omega$  that optimizes a given objective function  $g_0$ , which is often defined as compliance minimization or stiffness maximization. Introducing a density function defined in  $\Omega$  that assumes the value 1 in  $\Omega_{opt}$  and 0 in  $\Omega - \Omega_{opt}$ , therefore, the optimization problem can be written as

$$\begin{aligned} & \text{Min}_{\rho} g_0(\rho) \\ & \text{subject to:} \\ & \int_{\Omega} \rho d\Omega \leq \bar{V} \\ & \rho(\mathbf{x}) = 0 \text{ ou } 1, \forall \mathbf{x} \in \Omega \end{aligned} \quad (22)$$

In general, the topology optimization problem is treated by the discretization of the problem presented in Eq. (22), which is divided in  $N$  finite elements or subdomains. Taking  $\rho$  as constant function inside each finite element, so the problem shown in Eq. (22) can be written as

$$\begin{aligned} & \text{Min}_{\rho} g_0(\rho) \\ & \text{subject to:} \\ & V = \sum_{e=1}^N \rho_e v_e \leq \bar{V} \\ & \rho_e = 0 \text{ ou } 1, e = 1, \dots, N \end{aligned} \quad (23)$$

where  $\rho_e$  and  $v_e$  are the relative densities and volumes of the finite elements, respectively, and  $V$  is the final structure volume, Sigmund and Petersson [3].

The topology optimization is formulated as problem that searches for the best distribution of a given material quantity inside a reference domain. Since the work done by Bendsoe and Kikuchi [8], a

great part of the advances in topology optimization has been obtained through methodologies based on total strain energy minimization, which is directly related to the work done by external forces, Collet et al. [26]. Usually, this problem is denominated as structural compliance minimization, whose concepts are well-established, as presented by Collet et al. [26], Eschenauer and Olhoff [27], Rozvany [28] and Bendsøe and Sigmund [2].

In a continuum mechanics approach based on the finite element method, the compliance function represents twice the total strain energy. In addition, the design variables for the formulated problem is considered as the artificial material density of each element, which defines a volumetric fraction of a porous material and directly affects the constitutive material tensor, following the Voigt model,  $C_{ijkl}(\mathbf{x}) = \rho(\mathbf{x})C_{ijkl}^0(\mathbf{x})$ , which overestimates the effective material stiffness, once it assumes the uniformity of the strain tensor, Dvorak [29]. Therefore, the Voigt model defines the superior limit for the stiffness tensor of a composite material. Finally, considering an approach based on the micromechanics analysis of composite materials, the problem presented in Eq. (23) can be updated by the following formulation:

$$\begin{aligned} \min c(\boldsymbol{\rho}) &= \mathbf{d}^T \mathbf{K}(\boldsymbol{\rho}) \mathbf{d} \\ \text{subject to:} & \\ \frac{V(\boldsymbol{\rho})}{\bar{V}} &= f \\ \rho_e &= 0 \text{ ou } 1, \quad e = 1, \dots, N \end{aligned} \quad (24)$$

where  $c(\boldsymbol{\rho})$  is the structural compliance function,  $\mathbf{d}$  is the global vector of nodal displacements,  $V(\boldsymbol{\rho})$  and  $\bar{V}$  are the material volume and the reference domain volume, respectively,  $f$  is the prescribed volume fraction.

### 3.1 Solid Isotropic Material with Penalization (SIMP)

The optimization problem presented in Eq. (24) has a high complexity, so to find the solution algorithm we can modify the problem in two steps: relaxation and penalization of intermediate density values. First, the relaxation consists on increasing the design set, thus, the relative density, which in the original problem could assume only the values 0 or 1 according to presence of material, now can assume any real value between the interval 0 and 1 ( $0 < \rho \leq 1$ ), resulting in a design with different gray scales. Usually, we assume a minimum value for the relative density ( $\rho_{min}$ ), once the relative density must be different of 0 to avoid singularity in the stiffness matrix.

Second, according to Sigmund and Petersson [3], there are two different reasons to penalize the relative density intermediate values. The first reason refers to the post-processing of relaxation problem and the second point is to avoid the application of integer programming techniques in the solution of the optimization problem. The most popular method of penalization is the SIMP, which penalizes the intermediate densities with the purpose to avoid their presences in the optimal design. In this method, the material properties are assumed as constant inside each element and the design variables are the element relative density, which can be interpreted by volumetric fractions of porous materials that fill the element. Therefore, the effective stiffness tensor of each element is evaluated by the relative density raised by a certain power and multiplied by the solid material stiffness tensor. Differently of the problem presented in Eq. (24), which uses the Voigt model in the evaluation of the effective material stiffness tensor, Dvorak [29], in the SIMP method the effective constitutive tensor is evaluated by

$$C_{ijkl}(\rho) = \rho^p C_{ijkl}^0 \quad (25)$$

where  $C_{ijkl}^0$  is the solid material constitutive tensor and  $p$  is the penalization factor.

For the interpolation presented in Eq. (25), it is observed that  $C_{ijkl}(0) = 0$  and  $C_{ijkl}(1) = C_{ijkl}^0$ , which means that the final solution tends to present zero or one densities in all elements, inside a context of penalized intermediate values of relative density, resulting in a black and white design. According to Bendsøe and Sigmund [30], to topology optimization problems with volume constraint, the penalization factor must higher enough, normally  $p \geq 3$ , to have a black and white design. On this paper, it is suggested the adoption of the continued scheme of penalization, where the penalty factor

increases gradually from 1 to 4 avoiding the occurrence of local minima and obtaining black and white designs.

The optimization problem can be defined as

$$\begin{aligned} \min c(\boldsymbol{\rho}) &= \sum_{e=1}^N (\rho_e)^p \cdot \mathbf{d}_e^T \cdot \mathbf{k}_e^0 \cdot \mathbf{d}_e \\ \text{subject to:} & \\ \frac{V(\boldsymbol{\rho})}{\bar{V}} &= f \\ 0 < \rho_{min} &\leq \rho_e \leq 1 \end{aligned} \quad (26)$$

where  $\mathbf{d}_e$  is the local displacement vector,  $\mathbf{k}_e^0$  is the stiffness matrix for an element with an unit density and  $\rho_{min}$  is the minimum relative density (different of zero to avoid singularity).

### 3.2 Optimality Criteria (OC) method

A classical approach to the solution of structural optimization problem with a discretized domain is the OC method. Therefore, the OC method is a process often used to update iteratively the design variables and the Lagrange multipliers. Following the scheme suggested by Bendsøe and Sigmund [2], the heuristic update for the design variables can be stated as

$$\rho_e^{k+1} = \begin{cases} \max(\rho_{min}, \rho_e - m), & \text{if } \rho_e^k B_e^\eta \leq \max(\rho_{min}, \rho_e - m), \\ \rho_e^k B_e^\eta, & \\ \min(1, \rho_e + m), & \text{if } \max(\rho_{min}, \rho_e - m) < \rho_e^k B_e^\eta \leq \min(1, \rho_e + m), \\ \min(1, \rho_e + m), & \\ \rho_e^k B_e^\eta, & \text{if } \min(1, \rho_e + m) \leq \rho_e^k B_e^\eta \end{cases} \quad (27)$$

where  $k$  represents the iteration index,  $m$  is a positive moving limit,  $\eta$  is the damping factor and  $B_e$  can be expressed as

$$B_e = \frac{-\frac{\partial c}{\partial \rho_e}}{\lambda \frac{\partial f}{\partial \rho_e}} \quad (28)$$

where  $\lambda$  is the Lagrangian multiplier for volume constrained and is determined by a bisection method.

In the OC method, the damping factor performs an important role in the optimization process. A higher value of  $\eta$  can accelerate the convergence process to the optimal solution, however, this can cause oscillation during the optimization process. These difficulties during the convergence process are normally caused by displacements oscillations in the nodes that are in the low density regions of the structure during the iterative step, He et al. [31]. On the contrary, the adoption of lower values of  $\eta$  can avoid the divergence in the optimization algorithm, however, this can lead to small changes in the design variables, which can become the optimization process slow. Basically, the experience shows that this parameter should be kept as closer as possible from the optimal value of 1/2.

### 3.3 Evaluation of the compliance function for the standard finite volume theory

The concepts related to the topology optimization problem based on the compliance minimization are well established and there are several results that show its success, Collet et al. [26], as can be seen in Eschenauer and Olhoff [27], Rozvany [28] and Bendsøe and Sigmund [2]. In fact, the compliance function can be evaluated as twice the total strain energy caused by a displacement field  $\mathbf{u}$ , as follows

$$c(\mathbf{u}, \boldsymbol{\rho}) = 2U(\mathbf{u}, \boldsymbol{\rho}) = \iiint_{\Omega} \sigma_{ij}(\mathbf{u}, \boldsymbol{\rho}) \varepsilon_{ij}(\mathbf{u}) d\Omega = \iiint_{\Omega} \frac{1}{2} C_{ijkl}(\boldsymbol{\rho}) \varepsilon_{kl}(\mathbf{u}) \varepsilon_{ij}(\mathbf{u}) d\Omega \quad (29)$$

where  $\sigma_{ij}(\mathbf{u}, \boldsymbol{\rho})$  is the stress tensor,  $\varepsilon_{ij}(\mathbf{u})$  is the strain tensor,  $C_{ijkl}(\boldsymbol{\rho})$  is the stiffness tensor and  $\Omega$  is the analysis domain.

The equivalence between the total strain energy of a structure and the work done by external is satisfied only for the standard finite volume theory, once the differential equilibrium equations are

satisfied point-wise inside the subvolume. As a result, the compliance function can be rewritten as

$$c(\mathbf{u}, \boldsymbol{\rho}) = 2U(\mathbf{u}, \boldsymbol{\rho}) = 2W(\mathbf{u}, \boldsymbol{\rho}) = \iint_{S_\sigma} t_i u_i dS \quad (30)$$

where  $W(\mathbf{u}, \boldsymbol{\rho})$  is the work done by external forces,  $t_i$  is the traction vector acting on the boundary,  $u_i$  is the displacement vector and  $S_\sigma$  is the external surface where the external loadings are prescribed.

The compliance function for the standard formulation of the finite-volume, considering a structure discretized in  $N_q$  subvolumes, can be written as

$$c(\mathbf{u}, \boldsymbol{\rho}) = \sum_{q=1}^{N_q} 2U_q(\bar{\mathbf{u}}^{(q)}, \rho_q) = \sum_{q=1}^{N_q} 2W_q(\bar{\mathbf{u}}^{(q)}, \rho_q) = \sum_{q=1}^{N_q} \sum_{p=1}^4 \iint_{S_p^{(q)}} t_i^{(q,p)} u_i^{(q,p)} dS_p^{(q)} \quad (31)$$

where  $U_q(\bar{\mathbf{u}}^{(q)}, \rho_q)$  and  $W_q(\bar{\mathbf{u}}^{(q)}, \rho_q)$  are the local strain energy and the local work done, respectively, and  $\rho_q$  is the relative density of a generic subvolume  $q$ . Considering that the traction vector is constant in the subvolume faces and equals to the surface-averaged tractions acting on the faces, so,

$$c(\mathbf{u}, \boldsymbol{\rho}) = \sum_{q=1}^{N_q} \sum_{p=1}^4 \bar{t}_i^{(q,p)} \iint_{S_p^{(q)}} u_i^{(q,p)} dS_p^{(q)} = \sum_{q=1}^{N_q} \sum_{p=1}^4 \bar{t}_i^{(q,p)} \bar{u}_i^{(q,p)} L_p^{(q)} = \sum_{q=1}^{N_q} [\mathbf{L}^{(q)} \bar{\mathbf{t}}^{(q)}]^T \bar{\mathbf{u}}^{(q)} = \sum_{q=1}^{N_q} (\rho_q)^p [\mathbf{L}^{(q)} \mathbf{K}_{(8 \times 8)}^{(q)} \bar{\mathbf{u}}^{(q)}]^T \bar{\mathbf{u}}^{(q)} \quad (32)$$

where  $p$  is the penalty factor and  $\mathbf{L}^{(q)}$  is a matrix containing the subvolume face lengths, which can be expressed as

$$\mathbf{L}^{(q)} = \begin{bmatrix} \mathbf{L}_{(1)}^{(q)} & \mathbf{0} & \mathbf{0} & \mathbf{0} \\ \mathbf{0} & \mathbf{L}_{(2)}^{(q)} & \mathbf{0} & \mathbf{0} \\ \mathbf{0} & \mathbf{0} & \mathbf{L}_{(3)}^{(q)} & \mathbf{0} \\ \mathbf{0} & \mathbf{0} & \mathbf{0} & \mathbf{L}_{(4)}^{(q)} \end{bmatrix}, \text{ for } \mathbf{L}_{(p)}^{(q)} = \begin{bmatrix} L_p^{(q)} & 0 \\ 0 & L_p^{(q)} \end{bmatrix} \quad (33)$$

### 3.4 Mesh-independency filter

In order to avoid the occurrence of the numerical issues associated to the checkerboard pattern and the mesh dependency, especially in the approaches based on finite element method, it is used a filtering technique. It must be emphasized that this filter does not guarantee the existence of solution, however several numerical applications have shown that it can produce mesh-independent designs in practice, Sigmund [32]. This filtering technique modifies the elements or subvolumes sensitivities as follows

$$\frac{\partial c}{\partial \rho_e} = \frac{1}{\rho_e \sum_{f=1}^N \hat{H}_f} \sum_{f=1}^N \hat{H}_f \cdot \rho_f \cdot \frac{\partial c}{\partial \rho_f} \quad (34)$$

where  $\hat{H}_f$  is the convolution operator (weighting function) given as

$$\hat{H}_f = r_{min} - \text{dist}(e, f), \{f \in N | \text{dist}(e, f) \leq r_{min}\}, e = 1, \dots, N \quad (35)$$

where  $\text{dist}(e, f)$  is the distance between the center of element or subvolume  $e$  and the center of element or subvolume  $f$ , Sigmund [32].

## 4 Numerical results

On this section, three examples are analyzed to compare the efficiency of the new topology optimization approach based on the standard finite volume theory with the ones based on the finite element method analysis, employing the Q4 and Q8 elements. The studied examples are a cantilever beam subject to a concentrated load, a *Messerschmitt-Bölkow-Blom* (MBB) beam and a *Michell* structure. Through these examples, the numerical stability and efficiency of the finite volume theory are investigated. Besides, numerical aspects are investigated, such as number of iterations, processing

time and relative compliance. In order to avoid possible problems related to the local minima issue, the continued scheme of penalization is adopted, where the penalty factor increases gradually ( $\Delta p = 0.5$ ) from 1 to 4, as suggested by Talischi et al. [33]. Furthermore, a sensitivity filtering based on Eq. (34) is employed with the purpose to avoid mesh dependency, in the context of the finite volume theory, and checkerboard pattern, in the context of the finite element method, once Araujo et al. [25], Araujo [34] and Araujo et al. [35] have demonstrated the checkerboard free property of the finite volume theory.

The adopted convergence criterion is based on the maximum difference between successive steps of the relative material density function, thus, the loop finalizes when the following criteria is satisfied:

$$\max(|\rho^{k+1} - \rho^k|) < \text{TOL} \quad (36)$$

where  $\rho^k$  is the relative material densities vector of the previous step and  $\rho^{k+1}$  is the material relative densities vector of the current step. The adopted values for the numerical parameters of the model are:  $\text{TOL} = 0.01$ ,  $\rho_{\min} = 0.001$  and  $m = 0.5$ . To avoid divergence during the optimization process, the damping factor is adopted as closer as possible of  $1/2$ , since the non-convergence is avoided due to the oscillatory phenomenon. The employed computational environment, in terms of programming language and computer, can be described as: MatLab R2016a (64-bits)/Intel® Core™ i7 CPU 2.93 GHz/16.0 GB RAM/64-bits.

#### 4.1 Cantilever beam

The first analyzed example is a cantilever beam fixed in the left border and with a concentrated load in the middle of the right border, as shown in Figure 3. The proposed optimization problem consists on finding the minimum value for the structural compliance function, whose analysis domain and boundary conditions are given on Figure 3. In addition, the objective of this problem is to find the stiffest structure with a given volume of 40% of the total volume. In the model conception, consistent units for the physical and geometric parameters are adopted.

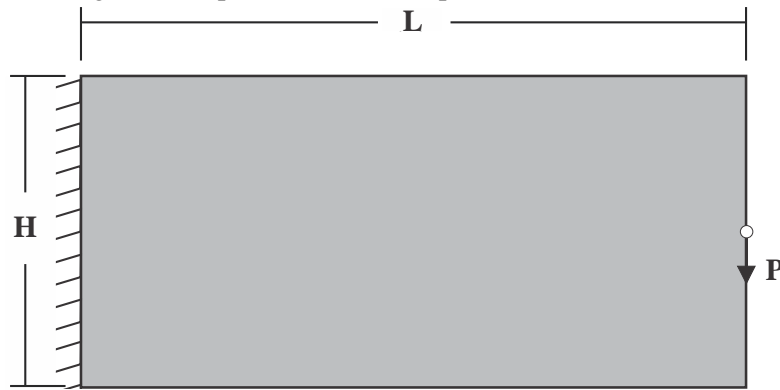


Figure 3. Cantilever beam.

In the scenario of the application of a sensitivity filter, the optimum topologies obtained by the finite volume theory and the finite element method are checkerboard free, as shown in Figure 4 and expected by Christensen and Klarbring [6]. Therefore, the applied sensitivity filter is able to avoid the occurrence of checkerboard regions in the optimum topology. From Figure 4, it can be also observed that the employed filtering technique can control better the solution dependency between different mesh sizes, however, it is registered a lower dependence when the finite element Q8 and finite volume theory are employed. On the contrary, when the finite element Q4 is employed, it is observed a higher dependence on the mesh size for the cantilever beam example.

Table 1 presents the results obtained for the overall convergence analysis employing the standard finite volume theory and the Q4 and Q8 elements of the finite element method. Basically, the number of iterations does not change substantially when the elements Q4 and Q8 are compared with the finite volume theory. On the other hand, the processing time varies depending on the approach, for instance,

the computational cost for the gradient-based optimization algorithm employing the finite element Q8, for the finest mesh, is 2.7 times higher than the same analysis employing the standard finite volume theory. At the same time, the analysis employing the finite element Q4 is approximately 1.6 times faster than the model that employs the zeroth order finite volume theory. The number of degrees of freedom (NDOF) explains a great part of the computational efficiency of the approaches based on the finite element Q4 and on the finite volume theory, once it defines the size of the global system of equations.

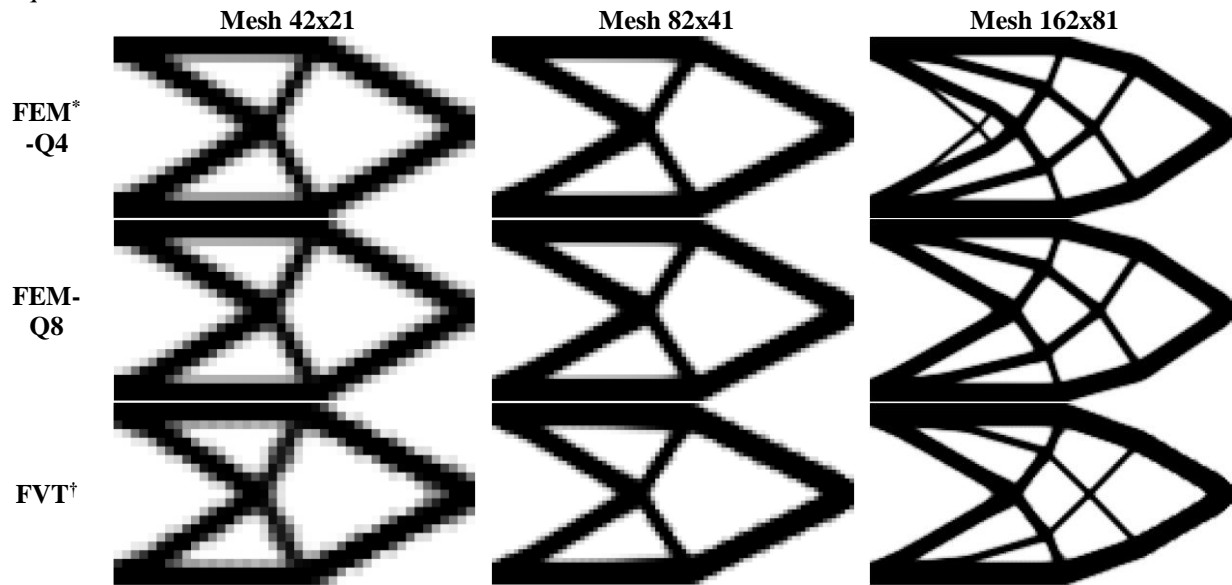


Figure 4. Optimum topologies for the cantilever beam analysis applying a sensitivity filtering.

Table 1. Convergence study for the cantilever beam applying a sensitivity filter.

Analysis	Mesh	NDOF	Number of Iterations	Processing Time (sec)	Relative Compliance
FEM-Q4	42x21	1892	117	21.58	1.0020
	82x41	6972	223	412.40	1.0008
	162x81	26732	298	7868.36	1.0121
FEM-Q8	42x21	5546	116	57.73	1.0000
	82x41	20666	167	1371.54	1.0000
	162x81	79706	312	34337.14	1.0000
FVT	42x21	3654	136	28.19	0.6654
	82x41	13694	194	487.68	0.8268
	162x81	52974	311	12744.41	0.8762

The relative compliance, shown in Table 1, can be calculated as follows

$$\text{Relative Compliance} = \frac{[c(\boldsymbol{\rho})]_{\text{FVT-Q8}}}{[c(\boldsymbol{\rho})]_{\text{Q8}}} \quad (37)$$

where  $[c(\boldsymbol{\rho})]_{\text{FVT-Q8}}$  is the compliance function value of the optimum topology obtained by the approach based on the finite volume theory recalculated using the element Q8 and  $[c(\boldsymbol{\rho})]_{\text{Q8}}$  is the compliance function value obtained by the approach based on the element Q8 of the finite element method, or

$$\text{Relative Compliance} = \frac{[c(\boldsymbol{\rho})]_{\text{Q4-Q8}}}{[c(\boldsymbol{\rho})]_{\text{Q8}}} \quad (38)$$

where  $[c(\boldsymbol{\rho})]_{\text{Q4-Q8}}$  is the compliance function value of the optimum topology obtained by the

\* Finite element method.

† Finite volume theory.

optimization algorithm employing the element Q4 recalculated using the element Q8.

The values obtained for the relative compliance indicate that the optimum structure obtained by the finite volume theory approach is stiffer than the approaches employing the finite element method, once the values obtained for FVT is lower than 1. Since the purpose of the topology optimization algorithm is to find the best material distribution inside a given domain and boundary conditions that maximizes the structural stiffness or minimizes the structural compliance, the optimum topologies obtained by the finite volume theory for the cantilever beam reveal to be better than the ones obtained by the finite element method.

#### 4.2 Messerschmitt-Bölkow-Blom (MBB) beam

The *Messerschmitt-Bölkow-Blom* (MBB) beam is shown in Figure 5, where consistent units for the physical and geometric parameters are adopted. Taking advantage of the symmetry, just half of the design domain is analyzed, employing boundary conditions that reflect this symmetry. In this case, the optimization problem consists on finding the minimum value for the structural compliance minimization subject to a volume constraint of 50% of the total structure volume.

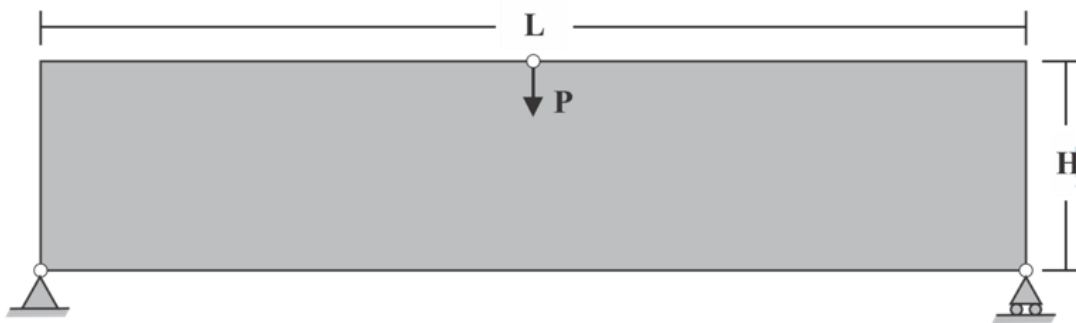


Figure 5. *Messerschmitt-Bölkow-Blom* (MBB) beam.

Figure 6 shows the optimum topologies obtained for the mesh sizes of 120x20, 240x40 and 360x60 for the analysis employing the elements Q4 and Q8 of the finite element method and the standard version of the finite volume theory. Basically, the optimum topologies, presented in Figure 6, are very similar for the three different approaches studied. Therefore, in the scenario of the sensitivity filter, the three different employed approaches are able to produce checkerboard free topologies with controlled mesh-dependency. However, as discussed previously, the approach based on the finite volume theory has checkerboard free property even when no filtering technique is employed, as shown by Araujo et al. [25], Araujo [34] and Araujo et al. [35]. On Table 2, the values obtained for the relative compliance show that basically there is any substantial change in the optimum topologies obtained for the three different employed approaches.

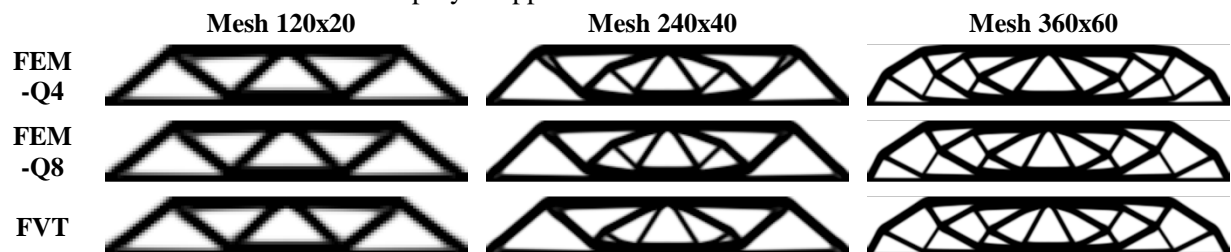


Figure 6. Optimum topologies for the MBB beam analysis applying a sensitivity filtering.

Table 2 shows the numerical results obtained for the convergence analysis of the MBB beam, employing the elements Q4 and Q8 of finite element method and the standard finite volume theory, respectively. The number of iterations varies highly in the case of the element Q4, which is almost half than the observed for the element Q8 and the finite volume theory, for finest mesh. In fact, this has contributed to the noticeable difference in the processing time, where the computational cost for the

finest mesh employing the element Q8 is 10.5 times higher than the same analysis employing the element Q4. At the same time, the approach based on the finite volume theory is 3.2 times slower than the same analysis employing the element Q4, for the finest mesh. The number of degrees of freedom and lower number of iterations for element Q4-based approach explains partially those differences in the computational cost.

Table 2. Convergence study for the MBB beam applying a sensitivity filter.

Analysis	Mesh	NDOF	Number of Iterations	Processing Time (sec)	Relative Compliance
FEM-Q4	60x20	2562	194	19.10	0.9989
	120x40	9922	267	530.38	1.0032
	180x60	22082	352	4845.16	1.0036
FEM-Q8	60x20	7522	172	107.38	1.0000
	120x40	29442	251	4065.47	1.0000
	180x60	65762	670	50714.64	1.0000
FVT	60x20	4960	165	19.91	1.0098
	120x40	19520	476	1623.34	1.0027
	180x60	43680	698	15289.46	1.0005

### 4.3 Michell structure

Figure 7 illustrates the analysis domain and the boundary conditions for the *Michell* structure employed in the analysis. In the model construction, it is adopted consistent units for the geometric and physical parameters. Considering the structure symmetry, only half of the reference domain is analyzed, thus, it is employed boundary conditions that reflect this symmetry. In this case, the optimization problem seeks to minimize the structural compliance function given a restriction of 40% of the total structure volume.

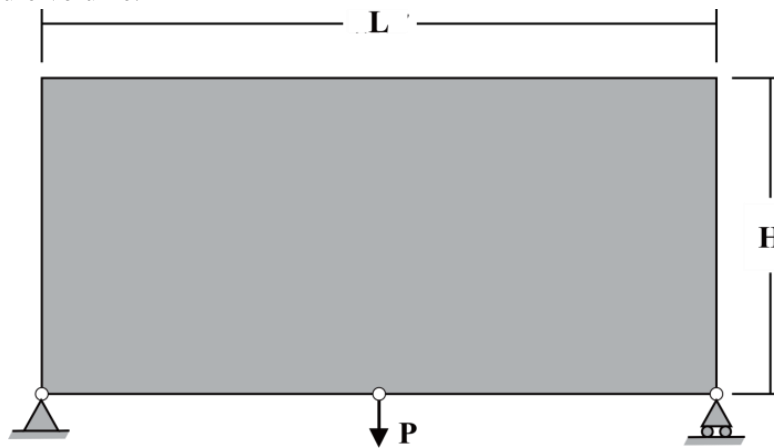


Figure 7. *Michell* structure.

Figure 8 presents the optimum topologies obtained for the meshes 60x30, 120x60 and 240x120, respectively, and employing the Q4 and Q8 elements of the finite element method and the standard finite volume theory. In the scenario of the application of the mesh-independent filtering, it is observed the absence of checkerboard regions and dependence on mesh size for all employed approaches. The optimum topologies obtained does not change substantially, only the optimum topology obtained for the finite volume theory employing a mesh size of 60x30 varies from the same employing the finite element method. However, the results for relative compliance, presented on Table 3, show that they are qualitatively almost the same.

The numerical results obtained for the convergence analysis of the *Michell* structure are presented on Table 3, which are obtained for the approaches based on the Q4 and Q8 elements of the finite element method and the standard finite volume theory, respectively. In this example, the number of iterations has an atypical behavior to the models employing the finite volume theory for mesh sizes of

30x30 and 120x120. In those cases, the number of iterations is higher than what is normally registered, which is basically the same for the three approaches studied, as obtained in Araujo et al. [25], Araujo [34] and Araujo et al. [35]. The adoption of a damping factor of 1/2 can explain partially these little instabilities registered for those specific two meshes, since the topology optimization algorithm applying the standard finite volume theory registers a great behavior when it is used a damping factor of 1/2.6, Araujo [34] and Araujo et al. [35].

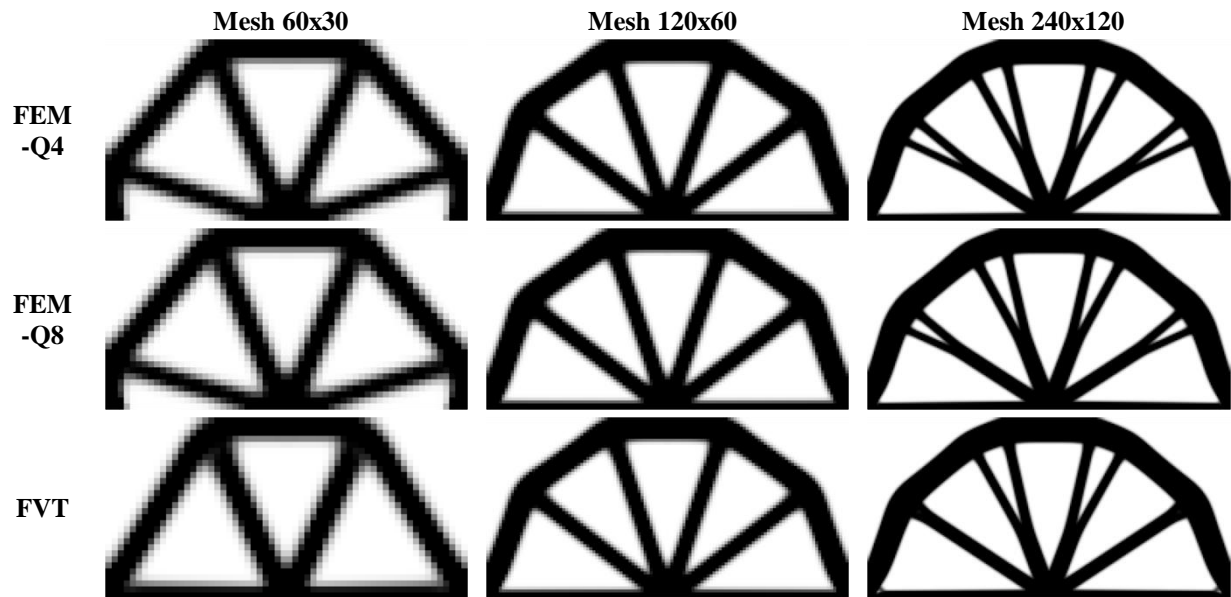


Figure 8. Optimum topologies for the *Michell* structure analysis applying a sensitivity filtering.

Table 3. Convergence study for the *Michell* structure applying a sensitivity filter.

Analysis	Mesh	NDOF	Number of Iterations	Processing Time (sec)	Relative Compliance
FEM-Q4	30x30	1922	129	10.87	0.9968
	60x60	7442	86	117.70	0.9989
	120x120	29282	253	6643.10	1.0014
FEM-Q8	30x30	5642	110	35.68	1.0000
	60x60	22082	87	715.77	1.0000
	120x120	87362	237	29685.74	1.0000
FVT	30x30	3720	171	22.22	1.0136
	60x60	14640	82	176.50	1.0019
	120x120	58080	373	15837.38	0.9974

The processing time, shown in Table 3, varies substantially depending on the employed approach. The computational cost for the Q8 element approach is 1.9 times higher than the observed for the finite volume theory. In addition, the Q4 element approach is 2.4 times faster than the same approach employing the finite volume theory. As in the previous examples, the number of degrees of freedom and iterations can explain a great part of those differences in the computational cost, since the NDOF defines the global system of equations and the number of iterations defines the length of time that the optimization process could take.

## 5 Conclusions

The topology optimization algorithm based on the standard finite volume theory has demonstrated to be efficient for the analyzed examples, especially in the case of the analyzed cantilever beam. In addition, the absence of numerical instabilities, such as the checkerboard pattern,

mesh dependence and local minima, shows the efficiency of the new numerical technique in the context of topology optimization of continuum elastic structures. A great part of its efficiency comes from the fact that this technique satisfies the kinematic and static continuity conditions in a surface-averaged sense through common faces between adjacent subvolumes, which means that the connections among subvolumes occur through edges instead nodes, as in finite element method. As a result, this induces the topology optimization algorithm based on the finite volume theory to have an intrinsic checkerboard free property.

The continued scheme of penalization, where the penalty factor is increased gradually from 1 to 4 with increments of 0.5, guarantees a gradual convergence for the overall optimization process and avoids the loss of uniqueness of the solution. In addition, the mesh-independent filtering is employed to solve problems related to the mesh-dependence and the length scale issues. Basically, the optimum topologies obtained by the proposed approach have presented less paths and larger lengths, especially in the case of the cantilever beam, which are desired features for manufacturing.

The damping factor of OC method is adjusted, depending on the adopted approach or the mesh size, with the intention to avoid possible divergences during the optimization process caused undesirable oscillations on the displacement field at the low density regions. The values adopted for the damping factor are as closer as possible of  $1/2$ , the need for changing this value is just observed for the coarsest meshes being more common in the Q8 element approach. The basic values instead of  $1/2$  are  $1/2.2$  and  $1/2.4$ .

In general, the optimum topologies obtained for the finite volume theory showed to be well-behaved, presenting topologies with great sharpness and clear material distribution. The implementation of a continued scheme of penalization guaranteed a gradual convergence for the overall process of optimization. The artificial microstructure of the SIMP approach allowed the penalization of low density regions, which made possible obtaining well-defined black and white designs. Finally, the results obtained justify the continuation of the investigation by exploring the different aspects of the finite volume theory, such as the local satisfaction of equilibrium equations and the kinematic and static continuity conditions being established in a surface-averaged sense.

## Acknowledgements

The authors acknowledge the financial support provided by the Brazilian federal agency CNPq.

## References

- [1] A. G. M. Michell. The limits of economy of material in frame structures. *The London, Edinburgh, and Dublin Philosophical Magazine and Journal of Science*, vol. 8, n. 47, pp. 589-597, 1904.
- [2] M. P. Bendsøe and O. Sigmund. *Topology Optimization: Theory, Methods and Applications*. Berlin: Springer-Verlag, 2003.
- [3] O Sigmund and J. Petersson. Numerical instabilities in topology optimization: A survey on procedures dealing with checkerboards, mesh-dependencies and local minima. *Structural Optimization*, vol. 16, n. 1, pp. 68-75, 1998.
- [4] A. Díaz and O. Sigmund. Checkerboard patterns in layout optimization. *Structural and Multidisciplinary Optimization*, vol. 10, n. 1, pp. 40-45, 1995.
- [5] O. Sigmund. Morphology-based black and white filters for topology optimization. *Structural and Multidisciplinary Optimization*, vol. 33, n. 4-5, pp. 401-424, 2007.
- [6] P. W. Christensen and A. Klarbring. *An Introduction to Structural Optimization*. Linköping: Springer Science & Business Media, 2009.
- [7] G. I. N. Rozvany. A critical review of established methods of structural topology optimization. *Structural and Multidisciplinary Optimization*, vol. 37, n. 3, pp. 217-237, 2009.
- [8] M. P. Bendsøe and N. Kikuchi. Generating optimal topologies in structural design using a homogenization method. *Computer Methods in Applied Mechanics and Engineering*, vol. 71, n. 2, pp. 197-224, 1988.

- [9] Y. Bansal and M. J. Pindera. Efficient reformulation of the thermoelastic higher-order theory for functionally graded materials. *Journal of Thermal Stress*, vol. 26, n. 11-12, pp. 1055-1092, 2003.
- [10] M. A. A. Cavalcante. *Modelagem Termomecânica Transiente de Estruturas de Materiais Compósitos pela Teoria de Volumes Finitos*. Master thesis in Civil Engineering – Federal University of Alagoas, Maceió, 2006.
- [11] M. A. A. Cavalcante, S. P. Marques and M. J. Pindera. Parametric formulation of the finite-volume theory for functionally graded materials – Part I: Analysis. *Journal of Applied Mechanics*, vol. 74, n. 5, pp. 935-945, 2007.
- [12] M. A. A. Cavalcante, S. P. Marques and M. J. Pindera. Parametric formulation of the finite-volume theory for functionally graded materials – Part II: numerical results. *Journal of Applied Mechanics*, vol. 74, n. 5, pp. 946-957, 2007.
- [13] M. A. A. Cavalcante, S. P. Marques and M. J. Pindera. Computational aspects of the parametric finite-volume theory for functionally graded materials. *Computational Materials Science*, vol. 44, n. 2, pp. 422-438, 2008.
- [14] M. A. A. Cavalcante and M. J. Pindera. Generalized finite-volume theory for elastic stress analysis in solid mechanics – part I: framework. *Journal of Applied Mechanics*, vol. 79, n. 5, pp. 051006, 2012.
- [15] M. A. A. Cavalcante and M. J. Pindera. Generalized finite-volume theory for elastic stress analysis in solid mechanics – part II: results. *Journal of Applied Mechanics*, vol. 79, n. 5, pp. 051007, 2012.
- [16] H. K. Versteeg and W. Malalasekera. *An Introduction to Computational Fluid Dynamics: The Finite Volume Method*. New York: Prentice-Hall, 2007.
- [17] M. A. A. Cavalcante, M. J. Pindera and H. Khatam. Finite-volume micromechanics of periodic materials: past, present and future. *Composites: Part B*, vol. 43, n. 6, pp. 2521-2543, 2012.
- [18] Y. Bansal. *Finite Volume Direct Averaging Micromechanics of Heterogeneous Media*. Master thesis in Applied Mechanics – University of Virginia, Charlottesville, 2005.
- [19] J. Aboudi, M. J. Pindera and S. M. Arnold. Higher-order theory for functionally graded materials. *Composites Part B: Engineering*, vol. 30, n. 8, pp. 777-832, 1999.
- [20] M. Gattu, H. Khatam, A. S. Drago and M. J. Pindera. Parametric finite-volume micromechanics of uniaxial, continuously-reinforced periodic materials with elastic phases. *Journal of Engineering Materials and Technology*, vol. 130, n. 3, pp. 031015-15, 2008.
- [21] H. Khatam, and M. J. Pindera. Parametric finite-volume micromechanics of periodic materials with elastoplastic phases. *International Journal of Plasticity*, vol. 25, n. 7, pp. 1386-1411, 2009.
- [22] H. Khatam, and M. J. Pindera. Plasticity-triggered architectural effects in periodic multilayers with wavy microstructures. *International Journal of Plasticity*, vol. 26, n. 2, pp. 273-287, 2010.
- [23] M. A. A. Cavalcante and M. J. Pindera. Generalized FVDAM theory for periodic materials undergoing finite deformations – part I: framework. *Journal of Applied Mechanics*, vol. 81, n. 2, pp. 021005, 2014.
- [24] M. A. A. Cavalcante and M. J. Pindera. Generalized FVDAM theory for periodic materials undergoing finite deformations – part I: results. *Journal of Applied Mechanics*, vol. 81, n. 2, pp. 021006, 2014.
- [25] M. V. O. Araujo, E. N. Lages and M. A. A. Cavalcante. Finite volume theory applied to topology optimization of continuum linear elastic structures. In: *Proceedings of XXXVIII Iberian Latin-American Congress on Computational Methods in Engineering*, Florianópolis, 2017.
- [26] M. Collet, M. Bruggi and P. Duysinx. Topology optimization for minimum weight with compliance and simplified nominal stress constraints for fatigue resistance. *Structural and Multidisciplinary Optimization*, vol. 55, n. 3, pp 839-855, 2017.
- [27] H. A. Eschenauer and N. Olhoff. Topology optimization of continuum structures: A review. *Applied Mechanics Reviews*, vol. 54, n. 4, pp. 331-390, 2001.
- [28] G. I. A. Rozvany. A critical review of established methods of structural topology optimization. *Structural and Multidisciplinary Optimization*, vol. 37, n. 3, pp. 217-237, 2009.
- [29] G. J. Dvorak. *Micromechanics of Composite Materials*. New York: Springer, 2013.
- [30] M. P. Bendsøe and O. Sigmund. Material interpolation schemes in topology optimization. *Archive of Applied Mechanics*, vol. 69, n. 9-10, pp. 635-654, 1999.

- [31] Q. He, Z. Kang and Y. Wang. A topology optimization method for geometrically nonlinear structures using with meshless analysis and independent density field interpolation. *Computational Mechanics*, vol. 54, n. 3, pp. 629-644, 2014.
- [32] O. Sigmund. A 99 line topology optimization code written in Matlab. *Structural and Multidisciplinary Optimization*, vol. 21, n. 2, pp. 120-127, 2001.
- [33] C. Talischi, G. H. Paulino, A. Pereira and I. F. Menezes. Polygonal finite element for topology optimization: A unifying paradigm. *International Journal for Numerical Methods in Engineering*, vol. 82, n. 6, pp. 671-698, 2010.
- [34] M. V. O. Araujo. *Teoria de Volumes Finitos Aplicada à Otimização Topológica de Estruturas Elásticas Contínuas*. Master thesis in Civil Engineering – Federal University of Alagoas, Maceió, 2018.
- [35] M. V. O. Araujo, E. N. Lages and M. A. A. Cavalcante. Free-checkerboard topology optimization using the generalized finite-volume theory. In: *Proceedings of the 7th International Symposium on Solid Mechanics*, São Carlos, 2019.

## Appendix

$$\mathbf{A}_{(8 \times 8)}^{(q)} = \begin{bmatrix} 0 & -\frac{1}{2}h_\gamma & 0 & \frac{1}{4}h_\gamma^2 & 0 & 0 & 0 & 0 \\ 0 & 0 & 0 & 0 & 0 & -\frac{1}{2}h_\gamma & 0 & \frac{1}{4}h_\gamma^2 \\ \frac{1}{2}l_\beta & 0 & \frac{1}{4}l_\beta^2 & 0 & 0 & 0 & 0 & 0 \\ 0 & 0 & 0 & 0 & \frac{1}{2}l_\beta & 0 & \frac{1}{4}l_\beta^2 & 0 \\ 0 & \frac{1}{2}h_\gamma & 0 & \frac{1}{4}h_\gamma^2 & 0 & 0 & 0 & 0 \\ 0 & 0 & 0 & 0 & 0 & \frac{1}{2}h_\gamma & 0 & \frac{1}{4}h_\gamma^2 \\ -\frac{1}{2}l_\beta & 0 & \frac{1}{4}l_\beta^2 & 0 & 0 & 0 & 0 & 0 \\ 0 & 0 & 0 & 0 & -\frac{1}{2}l_\beta & 0 & \frac{1}{4}l_\beta^2 & 0 \end{bmatrix} \quad (39)$$

$$\mathbf{a}_{(8 \times 2)}^{(q)} = \begin{bmatrix} 1 & 0 \\ 0 & 1 \\ 1 & 0 \\ 0 & 1 \\ 1 & 0 \\ 0 & 1 \\ 1 & 0 \\ 0 & 1 \end{bmatrix} \quad (40)$$

$$\mathbf{B}_{(8 \times 8)}^{(q)} = \begin{bmatrix} 0 & -C_{44}^{(q)} & 0 & \frac{3}{2}h_q C_{44}^{(q)} & -C_{44}^{(q)} & 0 & 0 & 0 \\ -C_{23}^{(q)} & 0 & 0 & 0 & 0 & -C_{22}^{(q)} & 0 & \frac{3}{2}h_q C_{22}^{(q)} \\ C_{22}^{(q)} & 0 & \frac{3}{2}b_q C_{22}^{(q)} & 0 & 0 & C_{23}^{(q)} & 0 & 0 \\ 0 & C_{44}^{(q)} & 0 & 0 & C_{44}^{(q)} & 0 & \frac{3}{2}b_q C_{44}^{(q)} & 0 \\ 0 & C_{44}^{(q)} & 0 & \frac{3}{2}h_q C_{44}^{(q)} & C_{44}^{(q)} & 0 & 0 & 0 \\ C_{23}^{(q)} & 0 & 0 & 0 & 0 & C_{22}^{(q)} & 0 & \frac{3}{2}h_q C_{22}^{(q)} \\ -C_{22}^{(q)} & 0 & \frac{3}{2}b_q C_{22}^{(q)} & 0 & 0 & C_{23}^{(q)} & 0 & 0 \\ 0 & -C_{44}^{(q)} & 0 & 0 & -C_{44}^{(q)} & 0 & \frac{3}{2}b_q C_{44}^{(q)} & 0 \end{bmatrix} \quad (41)$$

where  $C_{ij}^{(q)}$  are the components of the constitutive matrix.